CRYSTAL GROWTH & DESIGN

Article

Fully Inorganic Electrodeposition of Pure Aragonite Prismatic-like Textured Layers on Titanium Foils

C. Krauss, D. Chateigner, and O. Gil

Cryst. Growth Des., **2008**, 8 (12), 4378-4382 • Publication Date (Web): 30 September 2008

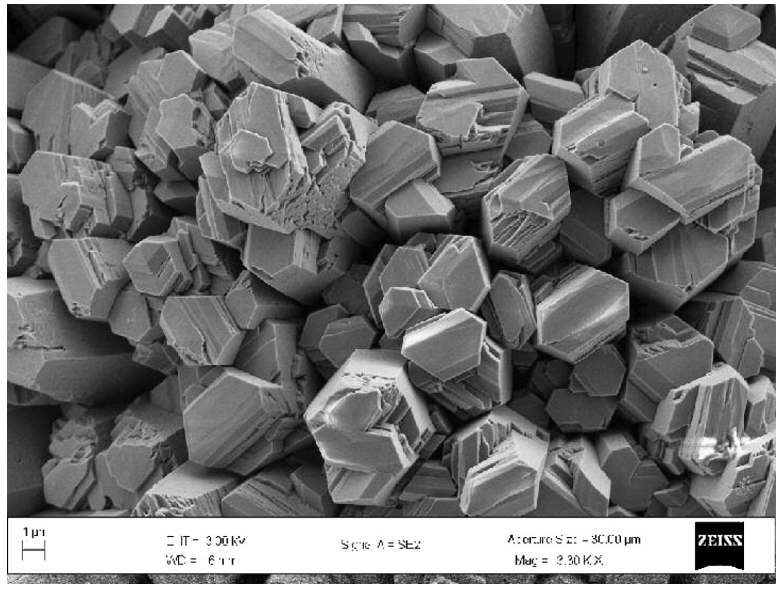

More About This Article

Additional resources and features associated with this article are available within the HTML version:

- Supporting Information
- Access to high resolution figures
- Links to articles and content related to this article
- Copyright permission to reproduce figures and/or text from this article

View the Full Text HTML

Crystal Growth and Design is published by the American Chemical Society. 1155 Sixteenth Street N.W., Washington, DC 20036

CRYSTAL GROWTH & DESIGN
2008
VOL. 8, NO. 12
4378–4382

Fully Inorganic Electrodeposition of Pure Aragonite Prismatic-like Textured Layers on Titanium Foils

C. Krauss,* D. Chateigner, and O. Gil

CRISMAT-ENSICAEN, CNRS UMR 6508, Université de Caen Basse-Normandie, Bd. M. Juin 14050 Caen, France

Received October 16, 2007; Revised Manuscript Received July 24, 2008

ABSTRACT: This work shows the capabilities of a specific method to synthesize pseudo-hexagonal prismatic-like layers on titanium foils without any organic matrix intervention, in constrast to mollusc shell growth. Using an electrochemical method of deposition, pure aragonite layers are obtained, which exhibit good texture strengths and pseudo-hexagonal crystals. The aragonite crystals grow with the *c*-axes orthogonal to the titanium foil surface without in-plane orientation, which resembles textures exhibited in nacre layers of some gastropods such as *Haliotis haliotis* with however lower texture strengths. It turns out that if organic materials can magnify textural characteristics in many aragonite-based layers, the inorganic influence is intrinsically large. This work will serve as a basis for mimicking synthetic hybrid layers by electrochemistry targeting osteoinductivity, with the view of substituting actual biocompatible, but inert, implants, and exemplifies the inorganic role played in the growth process of natural shells.

Introduction

Biomineralization of calcium carbonate-based living tissues remains controversially understood.[1] A tremendous amount of work has been dedicated to the understanding of mollusc shell growth. In mollusc shells, it is generally admitted, after the pioneering works of Weiner and co-workers,[2] that animal organic molecules (proteins, glycoproteins, polysaccharides, etc.) promote calcification and induce the development of strongly preferred orientations of the inorganic entity. For instance, in nacre, organization from the crystallography viewpoint is a matter of controversy. Crystallites orientation may be induced by the organic matter[3] or in a layer epitaxy growth,[4] but most probably crystals grow (and orient) by ionotropy onto the organic matrix.[5] Mollusc shells are mostly composed of aragonite and calcite layers, among which nacre layers have attracted much interest because of their excellent mechanical[6] and high osteoinductive[7,8] properties leading scientists to search for a mimic of its complex architecture.[9] Nacre is a biocomposite containing 95 vol% of quasi-hexagonal aragonite platelets,[10] 0.4−1.2 μm thick and 5−10 μm across arranged in a highly regular array, staggered in successive laminae and separated by a 5 vol% protein−polysaccharide complex-layered matrix.[11−14] However, we could not find in the literature composites with synthetic aragonite as quasi-hexagonal crystal shapes, although a lot of works are dedicated to the calcite crystal shape modifications or control by organic species and polyelectrolyte[15] and to the aragonite−calcite equilibrium changes under additive variations.[16]

In view of medical applications as orthopedics, working with titanium substrates appears to be essential because of its high strength, inertia, and immunity to corrosion by all body fluids and tissue. However, implants using pure titanium prostheses are subjected to bone resorbtion. Radiographic evidence was even reported indicating a loss of fixation at the implant−bone interface, probably due to accumulation of Ti particles acting on the bone-remodelling process and impacting both long- and short-term implant-fixation strengths.[17] On the other hand, Maya Indians of Honduras already used nacre for dental implants 2000 years ago.[18] In modern orthopedic medicine, aragonite of *Pinctada maxima* stimulates bone growth by human osteoblasts.[19]

We report here a specific technique to mimic hexagonal-like aragonite crystals in a textured manner on titanium substrates similar to those found in some molluscan shell layers. We use the capabilities of electrodeposition to coat medical-grade titanium substrates, in which parameter variation provides an easy monitoring of crystal shape and orientation, to demonstrate the at least partial nonorganic nature of crystal growing of related mollusc shell layers.

Experimental Section

Electrochemical Deposition. To obtain nacre-like deposits, we use a conventional three-electrodes cell monitored by a VersaStatII (Princeton Applied Research) potentiostat with a saturated calomel reference electrode and artificial seawater electrolyte (ASTM-D1141 standard). A platinum counter electrode ensures current flow and homogeneity on the ultrasonically cleaned titanium working electrode, using a specific protocol for reproducibility.[20,21] We used medical grade titanium (Ti6Al4V) as substrates for our deposits. Under application of a specific negative potential, oxygen and water reduction generate calcium carbonate precipitation on the titanium foil. Due to the high concentration of each component in the electrolyte and to the magnetic bar stirring, we can assume that the electrochemical deposition method used makes enough ions for continuous concentration of the chemical species which are involved in the depositing reactions at the electrolyte/working-electrode interface. This technique enables the monitoring of chemical reactions influencing the aragonite layer deposition on the working electrode. A typical intensity versus potential diagram (Figure 1) exhibits two main potential domains corresponding to oxygen reduction ($O_2 + 2H_2O + 4e^- \rightarrow 4OH^-$) and to water reduction ($2H_2O + 2e^- \rightarrow 2OH^- + H_2$). The oxygen reduction domain is optimal for calcium carbonate deposition because in this range a high pH zone is created near the titanium working electrode which generates precipitation. Calcium carbonate precipitates on the working electrode through the following reactions in aqueous environment: $NaHCO_3 \rightarrow Na^+ + HCO_3^-$, $CaCl_2 \rightarrow Ca^{2+} + 2Cl^-$, $HCO_3^- + OH^- \rightarrow CO_3^{2-} + H_2O$, $Ca^{2+} + CO_3^{2-} \rightarrow CaCO_3$ (solid). At negative potentials typically less than −0.35 V, water reduction occurs with H_2 release at the working-electrode surface favoring large film porosity and pull off. At potentials larger than −1 V, titanium reduction and oxidation take place.

Scanning Electron Microscopy. The microstructure of the layers was observed either using a XL 30 FEG Philips or Zeiss Supra 55 scanning electron microscope in the backscattering image mode at 10

* To whom correspondence should be addressed. E-mail: christopher.krauss@ensicaen.fr.

10.1021/cg701019c CCC: $40.75
Published on Web 09/30/2008

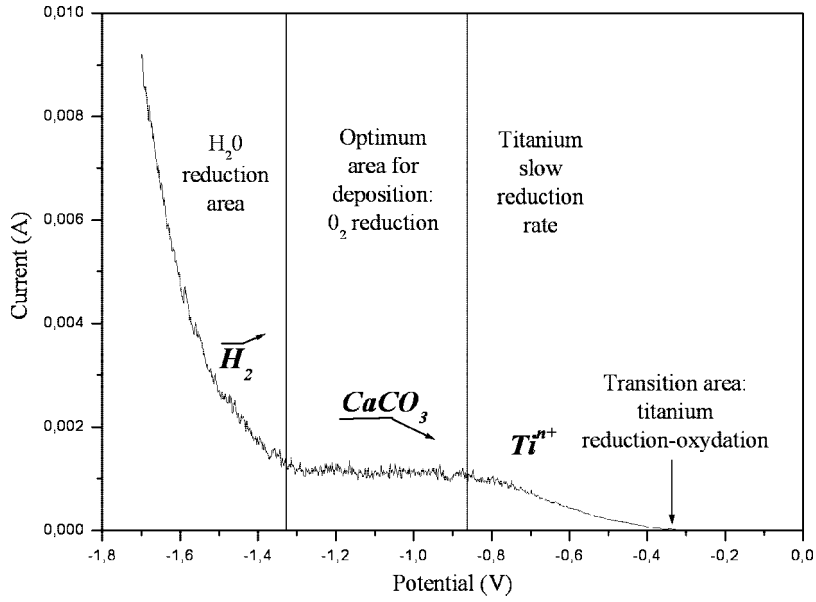

Figure 1. Intensity vs potential diagram used to adjust the experimental potentials around the frontier between water and oxygen reduction.

keV. To confirm the chemical composition of the deposits an Inca Oxford energy dispersive spectrometer was used.

Texture-Phase Analysis. For texture and phase analysis of the layers, we used a 4-circles diffractometer equipped with a 120° curved positioned sensitive INEL detector.[22] The texture scans were measured for the tilt angle χ in the 0°−60° range and in the 0°−360° range for the azimuth φ using increments of 5° for both angles. Using our diffractometer, a full 2θ diagram is measured for each (χ,φ) orientation of the sample, using 300 s of counting time. It results in 936 diagrams, each of them getting the same intensity as for a point-by-point measurement (with a point detector) with 300 s of integration at each point. The diagram set is then treated using the Rietveld-based software MAUD[23] within the combined analysis formalism.[24] Such an approach gives access to the mean deposit thickness, the structure, the phase fractions and texture of each phase and the crystallite mean sizes. Results for texture investigations are presented here as pole figures for the main aragonite crystal directions, that is, <100> and <001>. In the deposit pole figures, the normal to the film plane corresponds to the normal of the pole figures. In the *Haliotis* pole figures, the vertical, horizontal, and normal directions correspond to the growth, margin, and normal directions of the shell.[25]

Calcium carbonates crystallize in three allotropic forms: the much stable *calcite* form ($R\bar{3}c$, trigonal), the less stable *vaterite* ($P6_3/mmc$, hexagonal), and the metastable *aragonite* (*Pmcn*, orthorhombic). Because of the small difference between the Gibbs energies of calcite and aragonite ($\Delta G°_{c\rightarrow a} = -1$ kJ/mol), it becomes relatively easy to obtain only *Aragonite* by playing on the experimental parameters of electrodeposition as electrolyte temperature, composition, cell steering, etc.

Electrochemical Deposition of Aragonite. Each cited deposition parameters was optimized with a focus on oriented aragonite deposits. At high temperatures (higher as 50 °C) and high negative potentials (less than −1.5 V), the H_2 gaseous emission at the working interface induces high porosity of the deposit (Figure 2). After optimization of these parameters,[26] a typical potential of −1.4 V was chosen to operate deposition. A gross optimization of deposition conditions provides in 3 h typically 5 μm thick, pure aragonite deposits (Figure 3). Energy dispersive X-ray scattering analysis confirms the unique presence of calcium, carbon, and oxygen elements, in the $CaCO_3$ composition without all other elements from the seawater electrolyte such as Mg, and permits stirring adjust close to higher orientation in crystal growth. The increase of concentration of Mg in the electrolyte suppressed vaterite in the deposit and caused instability in calcite growth which induced preferentially aragonite deposit.[27] While usual cauliflower aragonite crystal shapes are observed for most of the deposition conditions (Figure 4a), interestingly hexagonal aragonite crystals are formed (Figure 4b,c) in the following condition ranges: (pH = [8.2, 8.3]; potential = [−1.45 V, −1.35 V]; $[MgCl_2]$ = [0.026 M, 0.029 M]; T = [38 °C, 45 °C]). The aragonite crystals are approximately 2 μm in width, appear as columnar growth at a small magnification (Figure 4b), and are homogeneously distributed at the surface of the titanium plate on several cm^2. However at large magnifications, the columns do show internal porosities at the 100 nm scale. Interestingly, these porosities are arranged parallel to the cross sections of the columns and look like cracks (Figure 4c,d). In the conditions used, the system is placed quite out of equilibrium, at relatively large temperatures and at a potential close to gaseous H_2 formation, which corresponds to aragonite metastable phase formation. Simultaneously, the Mg^{2+} species of the electrolyte prevent calcite stabilization in favor of aragonite. The equilibrium is shifted enough to create aragonite twins, known in this phase to promote quasi-hexagonal crystal shapes.[28,29] Crystals grow on the surface with hexagon planes parallel to the plate surface (Figure 4b) for most of them.

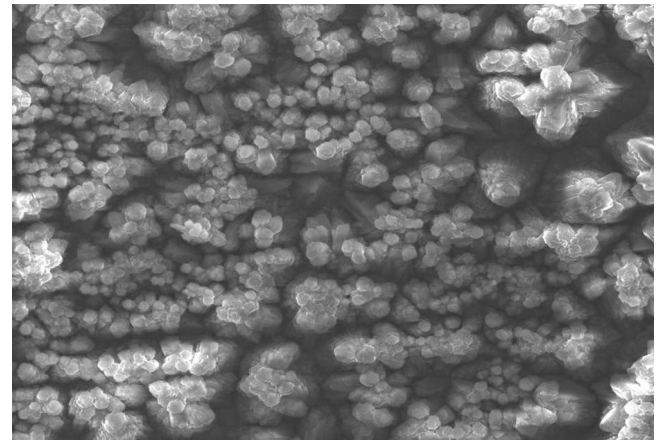

Figure 2. H_2 gaseous emission at the electrolyte/working-electrode interface induces high porosity and disorientation in crystal growth.

There is no clear speciation model to be described at the present time under our deposition conditions. Our method could result in processes similar to those described by Neville and Morizot.[30] These authors, in the context of cathodic protection, observed a first brucite-like layer at the interface with the steel electrode, before calcium carbonate crystallization occurs. Our first EDX analyses indeed revealed nucleation of an Mg-rich phase at the beginning of the deposition, but could not detect any Mg-integration in the latter aragonite crystals. However, we are using strongly negative potentials compared to these studies, and our titanium electrode could have a strong impact on the

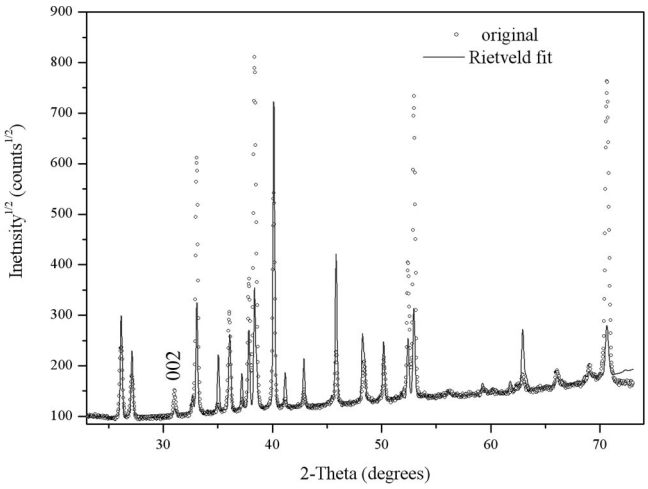

Figure 3. Experimental X-ray diffraction diagram (dots) of a typical nacre-like film. Note the enhanced (002) line compared to a perfect powder, indicating the pronounced (00*l*) orientation. Only lines from aragonite are observed. The diagram (line) corresponds to a Rietveld fit without texture correction.

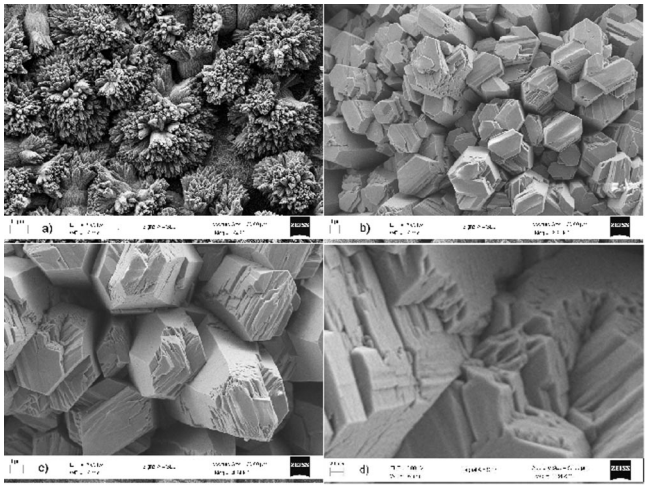

Figure 4. SEM backscattering images of aragonite deposits on titanium foils for (a) nonoptimized deposition conditions showing typically cauliflower-shaped aragonite, (b) optimized conditions with nacre-like pseudohexagonal-shaped crystals, and (c) same as (b) using a larger magnification.

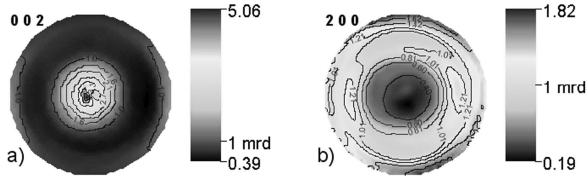

Figure 5. X-ray pole figures recalculated from the ODF. (a) (002) and (b) (200) pole figures of our film on Ti foil.

deposition process. Local Raman investigations will be performed to try to investigate further in this direction.

Results and Discussion

X-ray Characterization Results. A X-ray quantitative texture analysis[24] was performed on the films exhibiting crystals closest to hexagons (Figure 5a,b). Clearly, a strong texture is observed with *c*-axes of aragonite prominently oriented perpendicularly to the substrate plane, as seen on the {002} pole figure (Figure 5a). The (200) pole figure (Figure 5b) indicates that the *a*- and *b*-axes are randomly distributed around **c**, in a so-called <001> fiber texture. The pseudohexagons on the surface of the films then correspond to the (*a*,*b*) planes of aragonite, while the *c*-axes are perpendicular to the hexagons. Our film's texture reaches orientation densities around 5 times the random distribution (5 m.r.d.) along the fiber axis (maximum of the (001) pole figure). Such texture strengths are however far from aragonite orientation strengths in natural nacres of gastropods such as *Haliotis haliotis*. In these latter species, nacre exhibits highly intense diffraction peaks (Figure 6) with a more pronounced 002 line than on our films and some absent reflections because of the strong texture present in the layer. The X-ray quantitative texture analysis reveals a very large texture strength of this inner columnar nacre layer (Figure 6a,b), with a maximum orientation density of the (002) pole figure around 92 m.r.d.. Such a texture strength is among the strongest in mollusc shells.[25] Furthermore, the *a*- and *b*-axes of aragonite in this mollusc shell are, as in our films, at random around **c**, in a <001> fiber texture arrangement. From a textural point of view, electrochemical deposition can then provide strong mimicking of natural gastropod shells.

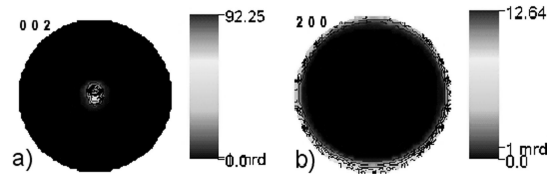

Figure 6. X-ray pole figures recalculated from the ODF (a) (002) and (b) (200) pole figures of the inner nacre layer of the gastropod *Haliotis haliotis*.

Discussion

Nacre layers are observed throughout Mollusca, exhibiting rather uniform crystal shapes and sizes. Following the terminology,[10] based on subunits observed in SEM section images, nacre can be classified in two different arrangements, columnar nacres (CN) or sheet nacres (SN) depending on the stacking mode of the individual tablets. Columnar nacre has platelets with coinciding centers, while in sheet nacre deposition takes place in a "brick-wall" pattern. Sheet nacres are mostly observed as inner layers of bivalves and monoplacophora. They exhibit the so-called "double-twinned" textures in the formers, with relatively small amounts of twins depending on the species, and fiber textures in the latter.[25,31] Columnar nacres are in majority observed in the inner layers of gastropods and cephalopods, with fiber textures and highly "double-twinned" textures, respectively. The textures observed in our films are then similar to the ones observed in columnar nacre of some gastropods (e.g., *Tectus niloticus, Haliotis haliotis*) and in sheet nacres of some monoplacophora (e.g., *Rokopella zographi*). The difference in texture strength, between our samples and natural nacres, can be associated to organic driven processes like the one giving a brick-wall sheet arrangement, though electrodeposition parameters could still be optimized to render larger texture strengths. Nevertheless the crystal shapes already are pseudohexagonal. It then seems that such crystal shapes do not need exclusively organic intervention but can be crystallized under out-of-equilibrium (large potential and cationic compositions) crystallization mechanism. This fact does not represent the first observation of the mineral influence on aragonite growth, since

for instance Checa et al.,[32] developed the "progressive organisation" model to partially account for *a*- and *b*-axes organization in bivalve nacres. Our texture and crystal morphology observation demonstrates there is a priori no need for organic material to play a role in the aragonite orientation in fiber-like gastropod textures (nacres and prismatic layers), except to enhance their texture strength. Furthermore, the intrinsic capability of aragonite to crystallize as twinned hexagons[33] is clearly exhibited in our purely inorganic films, twins being known to accommodate slightly larger energetic states of crystals.

Our elaboration conditions then provide enough perturbation to the equilibrium to promote twin formation, and smoothly enough to avoid cauliflower crystals. These observations would explain why organic amounts as small as 5 vol% are able to influence and control shell growths. Indeed, it might be difficult to understand how such smoothly textured organic material as observed by Weiner et al.[4] could induce such strong textures as observed in natural nacres, without inorganic capabilities to favor the process. Once nucleated on organic species, crystal growth takes place and the resulting crystal shapes behave depending on external conditions. These conditions can be purely thermodynamic (pressure, salinity, etc.) and/or provided by the organic entities (molecular nucleation sites, geometric configurations, etc.).[34] They can either promote specific crystal shapes (e.g., quasi-perfect nacre hexagons observed in large bivalves like *Pinctada margaritifera*), or restrict crystal growth inside organically constructed cells (e.g., nacre platelet domains variations as observed in *Haliotis* species[29]). Thermodynamic conditions are not believed generally to influence considerably shell growth. For instance, textures and crystal shapes of inner nacre layers of *Bathymodiolus thermophylus*[35] and *Mytilus edulis* are quite identical, although these two species live at considerably different pressures, which points toward a large organic influence. However, our experiments show that under given conditions, relatively small parameter changes (temperature, Mg concentration, etc.) can drastically modify both texture and crystal shapes and sizes. Since the observed lateral sizes of our synthetic aragonite columns are comparable to the ones found in natural species, one can argue there is a crystallographically intrinsic limited width of these columns that is used during shell growth by organic entities. Indeed, from an energetic point of view, it will become harder to accommodate twins when the lateral size of nacre columns increases, resulting either in creation of different columns or in different twinning arrangements of the columns as observed by Mutvei.[29] All the thermodynamically induced modifications are limited in magnitude (aragonite crystals grow generally acicular or as platelets, with or without twins) but can control ultrastructural variabilities imposed by organic materials in mollusc shells. Lastly, the aragonite prisms of Figure 4c show another aspect of the strong inorganic influence in aragonite growth. Each individual prismatic column appears segmented along its length at a larger magnification. The segments are delineated by cracks occurring every 0.3 μm along the length of the prismatic column which are typically about the same size as natural nacre tablets. Such resemblance is another aspect of the growing process of our films that goes toward the hypothesis of an inorganically driven crystallization in natural nacres. Such cracks accommodate partially twin-induced stresses along the columns. Once created, a given crack gives rise to free surfaces on which organic molecules could adsorb and permit further crystal nucleation. At this point, the adsorbed molecule can even induce a slightly different orientation of the next tablet, for instance, as the rotation around the *c*-axes observed from tablet to tablet in natural species.[36] In this new understanding of nacre development, organically driven crystallization relies on crack formation. However, this does not mean organic influence is absent. The latter still promotes much stronger global organization of crystals in between and inside nacre columns, but rather organic influence needs cracks to exist, at least along the columns. For instance, in calcite prism layers of bivalves such as *Crassotrea gigas*,[37] the prisms do not show any evidence of cracks, but are still macroscopically oriented.

Conclusion

Pure aragonite deposits on titanium substrates were elaborated using an electrochemical technique. The deposits are textured with their *c*-axes orthogonal to the titanium surface, *a*- and *b*-axes being at random around **c**, giving rise to <001> fiber texture patterns. Under given conditions, a pseudohexagonal cross-section of oriented aragonite rods is observed, due to the intrinsic aragonite twin symmetry. The observed textures of the deposits, together with the pseudohexagonal segmented prismatic crystal shapes, mimick prismatic natural layers found in gastropods columnar layers. The fully inorganic character of the deposition technique and the strong resemblance of the microstructures of the films with natural layers impose a stronger control of molluscan architectures by inorganic crystallization than previously understood.

References

(1) Mann, S. *Nature* **1988**, *332*, 119–124.
(2) Weiner, S.; Traub, W. In *Structural Aspects of Recognition and Assembly in Biological Macromolecules*; Balaban, M., Sussman, J. L., Traub, W., Yonath, A., Eds.; Balaban ISS: Rehovot, IS, 1981; pp 467−482.
(3) Weiner, S.; Traub, W. *FEBS Lett.* **1980**, *111*, 311–316.
(4) Weiner, S.; Talmon, Y.; Traub, W. *Int. J. Biol. Macromol.* **1983**, *5*, 325–328.
(5) Nassif, N.; Pinna, N.; Gehrke, N.; Antonietti, M.; Jäger, C.; Cölfen, H. *Proc. Natl. Acad. Sci. U. S. A.* **2005**, *102*, 12653–12655.
(6) Currey, J. D. *Proc. R. Soc. B* **1977**, *196*, 443–463.
(7) Lopez, E.; Vidal, B.; Berland, S.; Camprasse, S.; Camprasse, G.; Silve, C. *Tissue Cell* **1992**, *24*, 667–679.
(8) Atlan, G.; Balmain, N.; Berland, S.; Vidal, B.; Lopez, E. *C. R. Acad. Sci III-Vie* **1997**, *320*, 253–258.
(9) Sellinger, A.; Weiss, P. M.; Nguyen, A.; Lu, Y.; Assink, R. A.; Gong, W.; Brinker, C. J. *Nature* **1998**, *394*, 256–260.
(10) Caspi, E. N.; Pokroy, B.; Lee, P. L.; Quintana, J. P.; Zolotoyabko, E. *Acta. Crystallogr. B* **2005**, *61*, 129–132.
(11) Carter, J. G.; Clark, G. R. In Molluscs, notes for a short course; Bottjer, D. J.; Hickman, C. S.; Ward, P. D.; Broadhead, T. W.; *Department of Geological Sciences Studies in Geology*; University of Tennessee: Knoxville, 1985; pp 50−71.
(12) Nakahara, H. In *Mechanisms and Phylogeny of Mineralization in Biological Systems*; Suga, S.; Nakahara, H.; Springer: Berlin, DE, 1991; *Chapter 4.2*, pp 343−350.
(13) Nakahara, H. In *Biomineralization and Biological Metal Accumulation*; Westbroek, P.; Jong, E. W.; Reidel: Dordrecht, NL, 1983; pp 225−230.
(14) Cartwright, J.H. E.; Checa, A. G. *J. R. Soc. Interface* **2007**, *4*, 491–504.
(15) Wang, T.; Cölfen, H.; Antonietti, M. *J. Am. Chem. Soc.* **2005**, *127*, 3246–3247.
(16) Hosoda, N.; Sugawara, A.; Kato, T. *Macromolecules* **2003**, *36*, 6449–6452.
(17) Choi, M. G.; Koh, H. S.; Kluess, D.; O'Connor, D.; Mathur, A.; Truskey, G. A.; Rubin, J.; Zhou, D. X.; Sung, K. L. *Proc. Natl. Acad. Sci. U. S. A.* **2005**, *102*, 4578–4583.
(18) Bobbio, A. *Bull. Hist. Dent.* **1972**, *20*, 1–6.
(19) Silve, C.; Lopez, E.; Vidal, B.; Smith, D. C.; Camprasse, S.; Camprasse, G.; Couly, G. *Calcif. Tissue Int.* **1992**, *51*, 363–369.
(20) Barbiche, C.; Deslouis, C.; Festy, D.; Gil, O.; Refait, P.; Touzain, S.; Tribollet, B. *Electrochim. Acta* **2003**, *48*, 1645–1654.
(21) Deslouis, C.; Festy, D.; Gil, O.; Rius, G.; Touzain, S.; Tribollet, B. *Electrochim. Acta* **1998**, *43*, 1891–1901.

(22) Morales, M.; Chateigner, D.; Lutterotti, L.; Ricote, J. *Mater. Sci. Forum* **2002**, *408*, 113–118.
(23) Lutterotti, L.; Matthies, S.; Wenk, H. R. In *Proceedings of the Twelfth International Conference on Textures of Materials*; Szpunar, J. A., Ed.; NRC Research Press: Ottawa, CA, 1999; pp 1599−160.
(24) Chateigner, D. Combined Analysis: Texture-Structure-Phase-Stress-Reflectivity Characterisation Using X-ray and Neutron Scattering, 2004;http://www.ecole.ensicaen.fr/~chateign/texture/combinedanalysis.PDF.
(25) Chateigner, D.; Hedegaard, C.; Wenk, H. R. *J. Struct. Geol.* **2000**, *22*, 1723–1735.
(26) Krauss, C.; Chateigner, D.; Gil, O. Electrodeposition of nacre-like layers. *Electrochim. Acta*, submitted.
(27) Chen, T.; Neville, A.; Yuan, M. *J. Cryst. Growth* **2005**, *275*, 1341–1347.
(28) Bragg, W. L. In *Atomic Structures of Minerals*; Cornell University of Press: Ithaca, NY, 1937; pp 114−126.
(29) Mutvei, H. *The Mechanisms of Biomineralization in Animals and Plant*; Omori, M.; Watabe, N., Eds.; Tokai University Press: Tokyo, 1980; pp 49−56.
(30) Neville, A.; Morizot, A. P. *J. Cryst. Growth* **2002**, *243*, 490–502.
(31) Checa, A. G.; Rodriguez-Navarro, A. B. *Biomaterials* **2005**, *26*, 1071–1079.
(32) Checa, A. G.; Okamoto, T.; Ramírez, J. *Proc. R. Soc. London B* **2006**, *273*, 1329–1337.
(33) Fleming, S. D.; Parkinson, G. M.; Rohl, A. L. *J. Cryst. Growth* **1996**, *178*, 402–409.
(34) Checa, A. G.; Okamoto, T.; Ramirez, J. *Proc. R. Soc. B* **2006**, *273*, 1329–1337.
(35) Schaffer, T. E.; Ionescu-Zanetti, C.; Proksch, R.; Fritz, M.; Walters, D. A.; Almqvist, N.; Zaremba, C. M.; Belcher, A. M.; Smith, B. L.; Stucky, G. D.; Morse, D. M.; Hansma, P. K. *Chem. Mater.* **1997**, *9*, 1731–1740.
(36) Dalbeck, P.; England, J.; Cusack, M.; Lee, M. R.; Fallick, A. E. *Eur. J. Mineral.* **2006**, *24*, 601–609.
(37) Chateigner, D.; Morales, M.; Harper, E. M. *Mater. Sci. Forum* **2002**, *408−412*, 1687–1692.

CG701019C